Supplement of Atmos. Chem. Phys., 22, 6919–6935, 2022
https://doi.org/10.5194/acp-22-6919-2022-supplement

Supplement of

Molecular characteristics, sources, and formation pathways of organosulfur compounds in ambient aerosol in Guangzhou, South China

Hongxing Jiang et al.

Correspondence to: Jun Li (junli@gig.ac.cn)

Supplementary text

Measurements for $PM_{2.5}$ and Organics

A total of 55 $PM_{2.5}$ samples collected on prebaked quartz fiber filters once a week at Guangzhou from July, 2017 to June, 2018 (June–September: summer, October–November: fall; December–February: winter; March–May: spring) over a period of 24 h with a high-volume air sampler at a flow rate of 1 $m^3 \cdot min^{-1}$. Quartz fiber filters were preheated at 450°C for 6 h before used and weighed. After sampling, each filter was wrapped with prebaked aluminum foil, sealed. Before weighing again, the $PM_{2.5}$ samples were kept at constant temperature and humidity for 24 h. The difference between two weighing is the amount of collected $PM_{2.5}$. A punch of filter (1.5 cm^2) was used for carbon concentration measurement. The concentration of organic and elemental carbon were measured using an OC/EC analyzer (Sunset Laboratory,Inc.) following the NIOSH870 thermaleoptical transmittance (TOT) standard method. We converted OC to organic mass using a typical ratio of OM/OC of 1.8(Tolocka and Turpin, 2012). Detailed information about the analysis procedures of chemical tracers, and meteorological parameters have been described in previous studies(Jiang et al., 2021b; Jiang et al., 2021a) and are included in the Table S12. The organic tracers' analysis performed included levoglucosan, polycyclic aromatic hydrocarbons [PAHs], steranes, and hopenes, biogenic SOA tracers (isoprene-derived SOA, MTLs; monoterpene-derived SOA, MSOA), fatty acids, long-chain alkanes. Online data regarding temperature, RH, and NO_x were obtained from a local monitoring station. A gas filter correlation analyzer (Thermo Scientific, Model 48i) was used to observed the CO. SO_2 and O_3 was measured with the pulsed fluorescence analyzer (Thermo Scientific, Model 43iTLE) and the UV photometric analyzer (Thermo Scientific, Model 49i), respectively. NO and NO_2 were determined with a chemiluminescence instrument (Thermo Scientific, Model 42iTL). Meteorological parameters of temperature (T) and relative humidity (RH) were measured with a portable weather station (WXT520, Vaisala, Finland). The concentration of gas-phase OH radical was approximated from a nonlinear Pad• function, and the NO_x effects were considered.

Results from our previous work(Jiang et al., 2021b)**:** Seven-days backward trajectories were generated using the Hybrid Single Particle Lagrangian Integrated Trajectory (HYSPLIT) model. Trajectories were calculated for air masses starting from the sampling site at 500 m above ground level with 6-h intervals during the 24-h sampling period. All trajectories were classified into four clusters, including marine-origin air masses (summer monsoon period) from the Western Pacific and South East Asia regions, and continental-origin air masses (winter monsoon period) from Mongolia and Central Asia.

From the ^{14}C-based positive matrix factorization (PMF) analysis, we obtained 5 sources that contributed to the DOM: biomass burning (18%), fossil fuels combustion (32%), secondary inorganic nitrogen chemistry processes (20%), SOA formation associated with photochemical processes and waste combustion (7%), and SOA formation associated with isoprene-derived SOA and organic sulfates (22%). Fossil fuels combustion showed the highest average contribution to DOM but small changes in concentration across the year.

Biomass burning explained 18% of the DOM and showed a marked increasing trend from fall to winter. SOA factors were responsible for 50% of DOM mass, most of which was contributed by the factors that associated with secondary inorganic nitrogen chemistry processes, and isoprene-derived SOA and organic sulfates formations. DOM formed from secondary inorganic nitrogen chemistry processes showed higher concentrations in fall and winter, while DOM formed from secondary processes of isoprene and organic sulfates formations had lower concentrations in winter than in summer.

Measurements for particulate total sulfur and water-soluble sulfate

About 1~3 pieces of filters were cut using the steel punchers (1.5 cm^2) and then put it into clean tin boats directly. The sample were then crashed into a ball and further analyzed using elemental analyzer (Germany, elementar unicube) coupled with high sensitivity thermal conductivity detector in the CNS mode. The particle sulfur in $PM_{2.5}$ samples were calculated according to the calibration curve which were obtained by analyzing standard samples with different mass. The water-soluble sulfate or SO_4^{2-} was analyzed with ion-chromatography (761 Compact IC, Metrohm, Switzerland). A piece of filter (d=24 mm) was punched for each of collected field filter and dissolved into 12 mL distilled deionized water (≥18.2 Ω). Each sample was sonicated for 30 minutes allowing the solution reaching equilibrium. Then the filtrate was filtered through 0.22 μm PTFE membrane (Jinteng, China) and stored in a prewashed clean bottle at 4 ℃ until sample analysis. Detailed information about the analysis procedures were described in our previous studies (Jiang et al., 2020; Jiang et al., 2021b). Anions were separated on a Metrohm Metrosep A sup5-250 column with 3.2 mM Na_2CO_3 and 1.0 mM $NaHCO_3$ as the eluent and 35 mM H_2SO_4 for a suppressor. The injection loop volume for anion was 100 μL. The water-soluble sulfate-sulfur was calculated as 1/3 of the SO_4^{2-} concentration. The organic sulfur (Org-S) is calculated as the amount of sulfate-sulfur (SO_4^{2-}-S) subtracted from TS, and the ratio of organic sulfur to TS (Org-S/TS) can be calculated as:

$$\text{Org-S} = \text{TS} - \text{sulfate-sulfur} \quad \text{(S1)}$$

$$\text{Org-S/TS} = (\text{TS} - \text{sulfate-sulfur})/\text{TS} \quad \text{(S2)}$$

And the uncertainty of organosulfur fraction of total sulfur ($\delta_{OrgS/TS}$) for filter samples can be calculated using the following equation:

$$\delta_{OrgS/TS} = (RSD_{TS}^2 + RSD_{sulfate\text{-}sulfur}^2)^{1/2} * \text{sulfate-sulfur} / \text{TS} \quad \text{(S3)}$$

where RSD_{TS} and $RSD_{sulfate\text{-}sulfur}$ are the relative standard deviations determined for SO_4^{2-} and TS, respectively, both were 0.05 μg m^{-3} in this study.

Operating conditions for FT-ICR MS analysis

The ultrahigh-resolution FT-ICR-MS enables identification of complex atmospheric mixtures by giving accurate m/z value, and each peak was assigned to an ambiguous formula with <1ppm absolute mass error was achieved (Jiang et al., 2021a). Previous study has indicated that the OSs are readily ionized in the negative ESI mode, and most of them were observed only in the negative mode (Lin et al., 2012b; Kuang et al., 2016). Therefore, the negative ESI FT-ICR-MS analysis could provide a comprehensive understanding about the chemical composition of organosulfur compounds (OSCs) in atmosphere, though the molecular structures such as potential isomers were generally hidden behind a given m/z value.

A total of 55 $PM_{2.5}$ samples were used for negative ESI-FT-ICR MS analysis and each sample were ultrasonic extracted with methanol in cold water bath (Jiang et al., 2021a). Though we did not calculate the extraction efficiency of OSs with methanol in a cold-water bath, many previous studies have suggested that methanol could extracted more than 90% of OC both for filed samples or fresh biomass burning samples(Chen and Bond, 2010; Cheng et al., 2017; Huang et al., 2018). Considering OSs are polar compounds, and most of OSs can be dissolved in methanol(Ye et al., 2020). The potential artifacts resulted from extraction with methanol were not tested in this study. However, in a previous study, methanol was used as eluent to collected the humic-like substance for OSs characterization. Direct using methanol as extraction solvent to extract OSs was reported by Ye et al. (2020). All these studies have successfully characterized the OSs and made comparisons between ambient samples collected at different location. Therefore, we think that there might be small or no potential artifacts resulted from extraction with methanol. The methanol extracts were filtered with PTFE members and concentrated, and direct injected into a 9.4T solariX XR FT-ICR mass spectrometer (Bruker Daltonik GmbH, Bremen, Germany) in negative ESI modes at a flow rate of 180 $\mu L\ h^{-1}$ (Jiang et al., 2021a; Jiang et al., 2020). Detailed operating conditions are set as: capillary voltage and capillary column end voltage for the negative ESI-FT-ICR MS analysis were set to 4.5 kV and −500 V, ions were accumulated in a hexapole for 0.65s, and the conditions of Octupole were set as 5 MHz and 350 V of peak to-peak (Vp-p) radio frequency (RF) amplitude. An argon-filled hexapole collision pool was operated at 2 MHz and RF amplitude of 1400 Vp-p, in which ions were accumulated for 0.02 s. The optimized mass for quadrupole (Q1) was 170 Da with the time of flight is 0.65ms. The mass range was set as150–800 Da, and a total of 128 continuous 4M data FT-ICR transients were co-added to enhance the signal-to-noise ratio and dynamic range. Field blank filters were processed and analyzed following the same procedure to detect possible contamination. All mass spectra were calibrated externally with arginine clusters in negative ion mode using a linear calibration. The final spectrum was internally recalibrated with typical O_2 class species peaks using quadratic calibration in DataAnalysis 5.0 (Bruker Daltonics). A typical mass-resolving power (m/Δm50 %, in which Δm50% is the magnitude of the mass spectral peak full width at half-maximum peak height) >450 000 at m/z 319 with <0.3 ppm absolute mass error was achieved. In this study, three duplicate representative aerosol samples were analyzed at the beginning, middle, and end of the analysis to test the reproducibility of sample extraction, the peak detection of the method, and the molecular formula assignment procedures. Pearson's correlation analysis of the relative intensities of all molecules between duplicates confirmed the high level of reproducibility of the selected samples (r = 0.98) (Jiang et al., 2021a).

FT-ICR MS data processing

A custom software was used to calculate all mathematically possible formulas for all ions with a signal-to-noise ratio above 4 using a mass tolerance of ±1ppm. The compounds assigned as $C_cH_hO_oN_nS_s$ with s = 1, 2 will be collectively referred to as organosulfur compounds (OSs) including CHOS (n = 0) and CHONS (n = 1,2). The identified formulas containing isotopomers (i.e., ^{13}C, ^{18}O or ^{34}S) was not discussed. The intensity-weighted elemental ratios such as O/C, H/C, O/S were calculated as described in previous study (Jiang et al., 2021a). The double bond equivalent (DBE) is calculated using the equation:

$$DBE = (2c+2-h+n)/2 \quad \text{(S4)}$$

Additionally, the modified index of aromaticity equivalent (Xc) which was considered as a better index to describe potential monocyclic and polycyclic aromatic compounds with S atoms, were also calculated using the flowing equation (Ye et al., 2020; Yassine et al., 2014):

$$X_c = \frac{3[DBE-(m\times o+n\times s)]-2}{DBE-(m\times o+n\times s)} \quad \text{(S5)}$$

Where m and n correspond to the fraction of oxygen and sulfur involved in the π-bond structure of the compound, respectively. If DBE ≤ (m×o+n×s), then Xc=0 is assumed. For chemical classes including alchohol, ether, sulfide, disulfide, sulfinic and sulfonic acids, m=n=0 should be used. And for chemical classes including carboxylic acid, ester and nitro, m=0.5 was adopted. Assuming the sulfur atom of organosulfur molecule exists in a sulfate group (R-OSO_3H) or a sulfonate group (R-SO_3H), the organosulfur molecule can be converted into a virtual organic carbon molecule by replacing -OSO_3H with -OH (or -SO_3H with -H). Considering negative ESI-FT-ICR MS analysis was performed, and the negative ESI mode is sensitive to compounds containing carboxylate, sulfonate and nitro groups. Thus, the calculation for Xc of organosulfur compounds can be simplified as (Ye et al., 2020):

$$X_c = \frac{3[DBE-0.5\times(o-4)]-2}{DBE-0.5\times(o-4)} \quad \text{(S6)}$$

We rounded 0.5×(*o*–4) down to the next lower integer if *o* is an odd number. A value of Xc≥2.5000 was supposed as the unambiguous minimum criterion for the presence of an aromatic structure. Xc≥2.7143, 2.8000, 2.8333, 2.9231 were considered as the thresholds for molecules containing cores of naphthalene, anthracene, pyrene and ovalene, respectively.

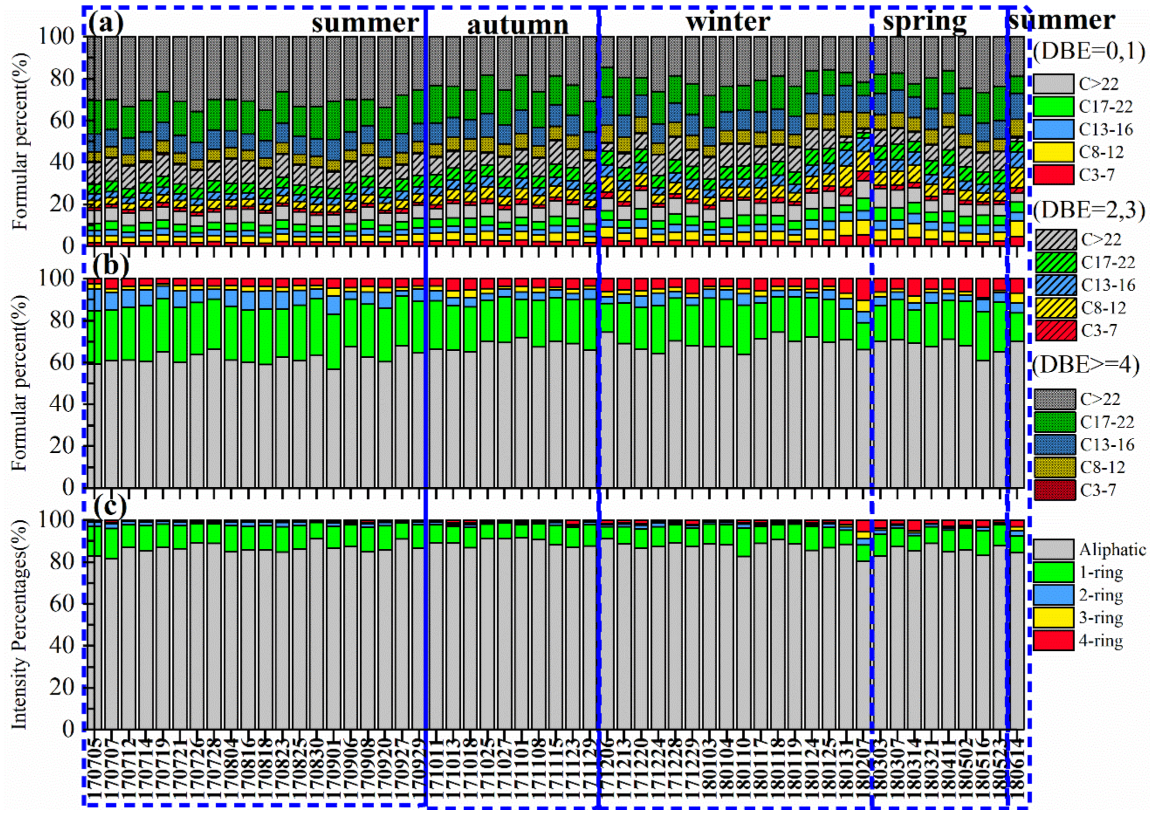

Figure S1. (a) Formular number percentages of each subgroup which divided based on the DBE value and the length of carbon skeleton in the CHOS formulas; (b) and (c) Intensity percentages and formular number percentages of each subgroup which divided based on the Xc value of formulas.

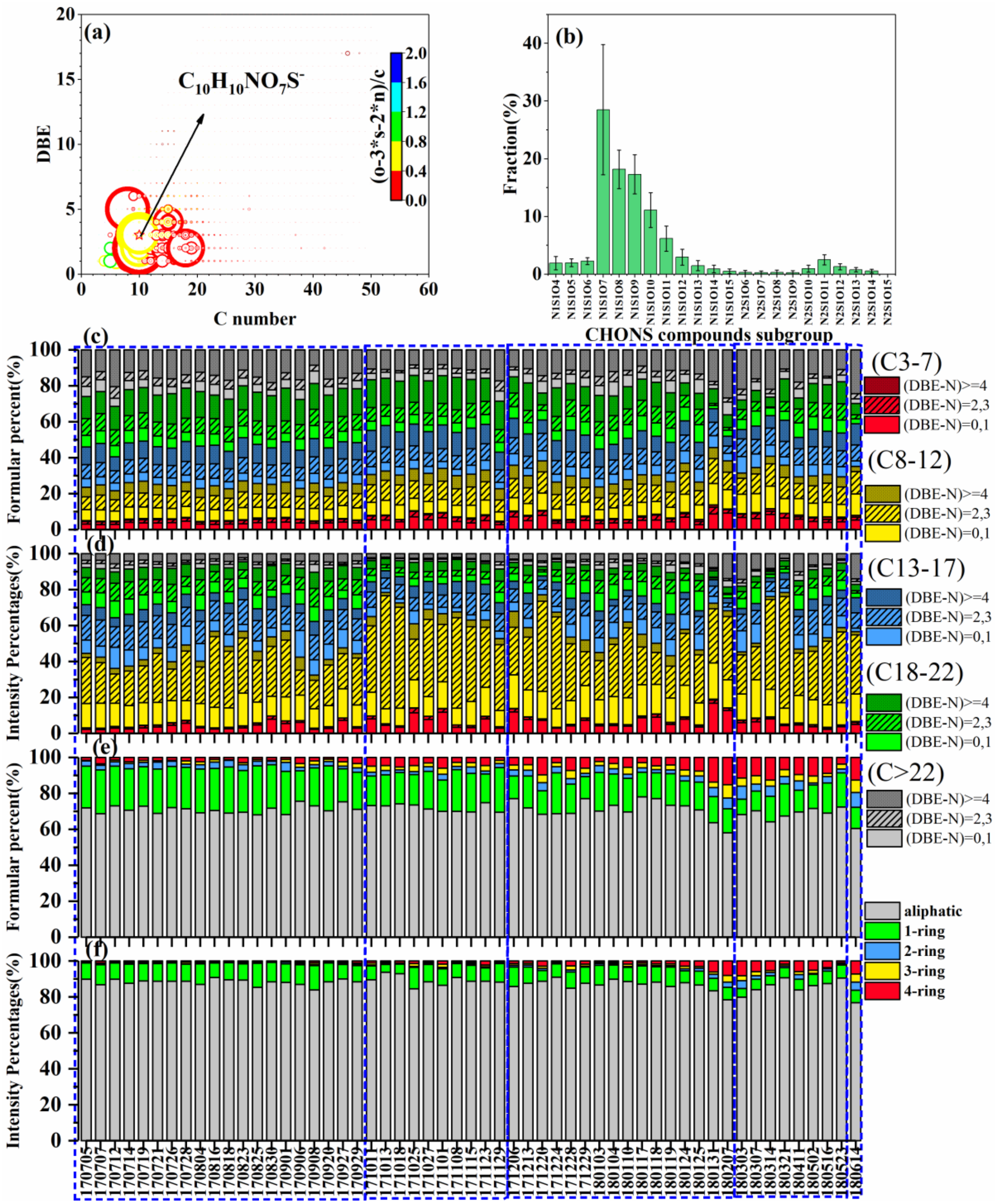

Figure S2. Molecular distribution of CHONS compounds detected by FT-ICR MS for the sample set collected in Guangzhou. (a) Double bond equivalent (DBE) vs C number for all the CHONS compounds of all samples. The color bar and marker size denote the number of oxidation state and the average sum-normalized relative peak intensities of the compounds; (b) Classification of CHONS species into different subgroups according to the numbers of S and O atoms in their molecules; (c) and (d) Intensity percentages and formular number percentages of each subgroup which divided based on the DBE value and the length of carbon skeleton in the formulas; (e) and (f) Intensity percentages and formular number percentages of each subgroup which divided based on the Xc value of formulas.

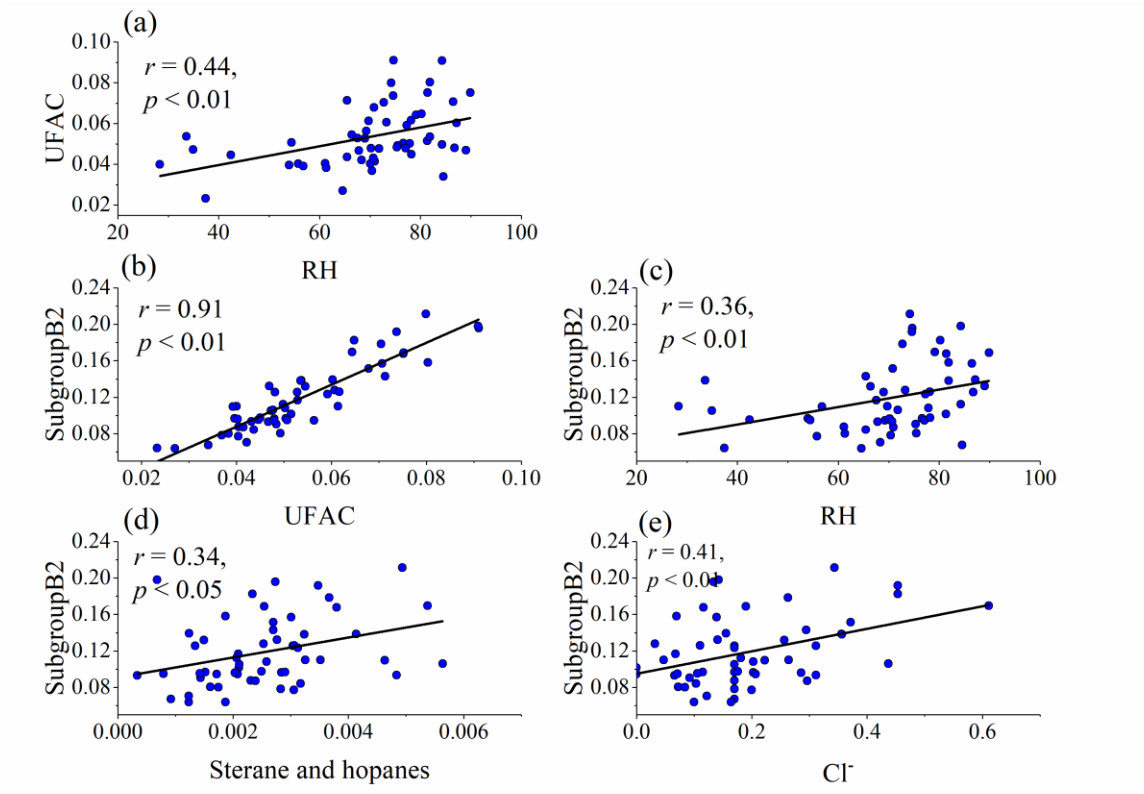

Figure S3. Significant correlations between (a) the sum-normalized intensity of OSs form potential unsaturated fatty acid compounds (UFAC) and RH, and the sum-normalized intensity of OSs classified into the subgroupB2 (with DBE⩽2, C>8, 3<O<7 for CHOS and DBE⩽2, N=1, C>8, 6<O<10 for CHONS compounds) and (b) UFAC, (c) RH, the concentrations of (d) sterane and hopanes, (e) Cl^-.

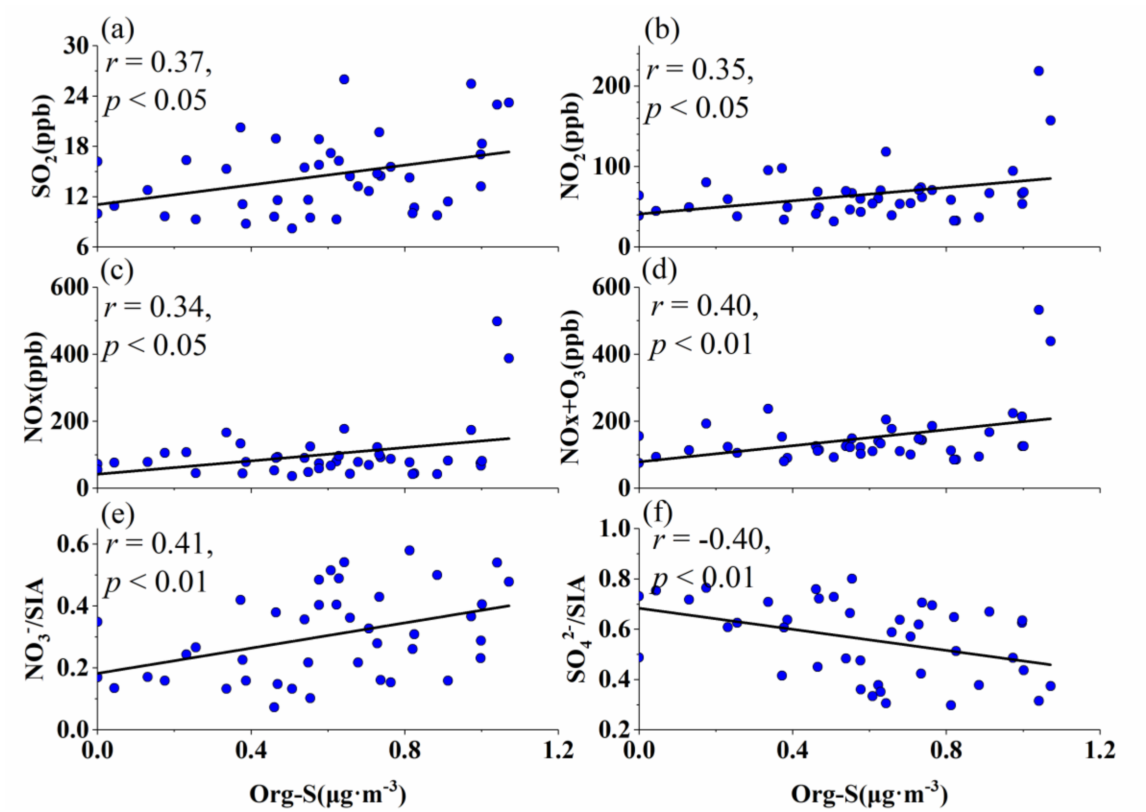

Figure S4. Significant correlations between the concentration of Org-S and (a) SO_2, (b) NO_2, (c) NO_x, (d) NO_x+O_3, (e) NO_3^-/SIA, (f) SO_4^{2-}/SIA.

Table S1. Summary of the concentration of organosulfur (Org-S) and fraction in total particulate sulfur (TS), organic carbon (OC), organic matter (OM), and $PM_{2.5}$ mass reported in recent studies (OS denotes organosulfates).

Sites		Org-S (μg/m^3)	Org-S/TS	Org-S /OC	OrgSs /OM	Org-S /PM	Ref.
Guangzhou		0.04−1.1 (0.6)	0.07−50% (33%)		11−89% (42%)	0−3% (1.4%)	This study
Four Asian sites	Maldives	0.3 (OS)	2.1%	4.4%		0.9%(OS)	(Stone et al., 2012)
	Gosan	0.1 (OS)	1.1%	3.5%		0.6% (OS)	
	Singapore	0.3 (OS)	2.5%			1.4% (OS)	
	Lahore	0.9−2 (OS)	5.9−7.7%	0.4−0.8%		0.7−0.9% (OS)	
Continental aerosol						4% (OS)	(Hawkins et al., 2010)
Whistler, British Columbia						< 1%(OS)	(Schwartz et al., 2010)
Polar region			6%		9−11%(OS)		(Frossard et al., 2011)
Kpuszta, Hungary		0.02−0.09	6−12%		8−50 % (OS)		(Luk´Acs et al., 2009)
		0.33	20%		30 %(OS)		(Surratt et al., 2008)
Fairbanks, Alaska				1.3% 0.7−2.1% (OS)		0.8% 0.6−1.0% (OS)	(Shakya and Peltier, 2013)
Eight sites in U.S.		up to 0.07		10−13%		1−3%	(Shakya and Peltier, 2015)
12 sites in U.S.		0.1−1.4		1−20% (OS)	5−10% (OS)		(Tolocka and Turpin, 2012)
Mt Kleiner Feldberg in central Germany			40%				(Vogel et al., 2016)
21 sites in U.S.		<0.0376 to 0.3					(Dombek et al., 2020)
U.S. (eastern and western, composite)		0.3±0.2 to 0.5±0.2	16±3 to 17±5				(Chen et al., 2021)

Table S2. Summary of the calculated molecular characteristics of organosulfur compounds groups detected in the yearlong sample set.

Group	Subgroup	For sample										For OrgSs formulas set[b]	
		Number of formulas	% of total OrgSs[a] formulas	% of total OrgSs Intensity	Number of formulas with *o*/(4*s*+3*n*) ≥ 1	% of formulas with *o*/(4*s*+3*n*) ≥ 1	MW	H/C	O/C	O/S	DBE	Number of formulas	% of formulas with o/(4s+3n) ≥ 1
CHOS	$CHOS_1$	406-2199	57(50-67)	70(56-80)	389-2143	97(94-99)	349(305-378)	1.78(1.72-1.84)	0.52(0.40-0.67)	6.7(5.8-7.7)	2.64(2.22-2.90)	5664	5256(93%)
	$CHOS_2$	82-291	6(4-12)	2(1-6)	35-149	46(31-63)	583(519-649)	1.50(1.30-1.66)	0.33(0.21-0.50)	3.8(3-4.3)	7.80(5.78-9.38)	3722	2017(54%)
	Total	**498-2383**	**64(58-73)**	**72(59-84)**	**432-2262**	**92(87-95)**	**355(315-389)**	**1.77(1.72-1.83)**	**0.52(0.40-0.68)**	**6.7(5.7-7.7)**	**2.77(2.39-3.50)**	**9386**	**7273(77%)**
CHONS	$CHON_1S$	190-1344	31(22-35)	26(15-37)	159-1177	83(75-89)	366(325-399)	1.72(1.65-1.77)	0.71(0.63-0.84)	8.4(7.5-9.5)	3.46(3.10-4.45)	4397	3253(74%)
	$CHON_2S$	40-247	5(2-10)	2(1-6)	25-227	78(48-94)	455(390-553)	1.69(1.42-1.80)	0.90(0.61-1.35)	11.0(9.7-11.9)	4.85(3.49-8.06)	2215	1357(61%)
	Total	**269-1591**	**36(27-42)**	**28(16-41)**	**202-1389**	**82(70-89)**	**373(331-405)**	**1.72(1.62-1.76)**	**0.72(0.63-0.85)**	**8.6(7.7-9.7)**	**3.56(3.15-4.89)**	**6612**	**4610(70%)**

a OrgSs: Organosulfur Compounds

b OrgSs formulas set denotes the all organosulfur compounds detected in all samples.

Table S3. Comparison of O/C and H/C ratios of CHOS compounds in this study and other studies.

Sample/type	Site/type		Extraction solution	O/C	H/C	Instrument	Ref.
$PM_{2.5}$	CHOS		Methanol	0.52±0.07	1.77±0.03	FT-ICR MS	This study
Rainwater	Northeastern United States		Water	1.3±0.8	1.9±0.5	FT-ICR MS	(Altieri et al., 2009)
$PM_{2.5}$	Pearl River Delta		Water	0.55 ± 0.17	1.67±0.31	Orbitrap MS	(Lin et al., 2012a)
$PM_{2.5}$	Cambridge	winter	Water and acetonitrile	0.47	1.47	Orbitrap MS	(Rincón et al., 2012)
		summer		0.66	1.50		
Cloud	Colorado		Water	0.43±0.09	1.41±0.27	FT-ICR MS	(Zhao et al., 2013)
				0.42±0.05	1.41±0.17		
PM (0.18-1.8 μm)	California	after midnight		0.87±0.09	1.7±0.05	Orbitrap MS	(O'brien et al., 2014)
		morning		0.93±0.1	1.8±0.1		
		afternoon		0.82±0.09	1.8±0.05		
		before midnight		0.88±0.05	1.8±0.0		
TSP	Virginia		Water	0.47±0.23	1.46±0.35	FT-ICR MS	(Willoughby et al., 2014)
			Pyridine	0.49±0.31	1.54±0.38		
			Acetonitrile	0.49±0.32	1.42±0.36		
$PM_{2.5}$	Beijing	Hazy	DCM	0.49±0.26	1.55±0.41	FT-ICR MS	(Jiang et al., 2016)
		Clear		0.62±0.34	1.74±0.34		
		Hazy	Water	0.65±0.28	1.64±0.37		
		Clear		0.75±0.37	1.82±0.26		
$PM_{2.5}$	Wuhan	Winter	Methanol	0.37±0.25	1.68±0.44	Orbitrap MS	(Wang et al., 2016)
		Summer		0.39±0.23	1.75±0.36		
	Nanjing	Summer		0.43±0.32	1.68±0.41		
	Shanghai	Winter		0.40±0.29	1.68±0.46		
		Summer		0.47±0.31	1.68±0.42		
$PM_{2.5}$	Shanghai	Spring	Acetonitrile	0.2	1	Orbitrap MS	(Wang et al., 2017)
		Summer		0.6	1.1		
		Fall		0.4	1.2		
		Winter		0.2	1.3		
$PM_{2.5}$	Mainz	low-pollution	Acetonitrile-water	0.78	1.66	Orbitrap MS	(Wang et al., 2018)

	Beijing	low-pollution		0.63	1.81		
		high-pollution		0.51	1.74		
Cloud	France		Water	0.3	1.52	FT-ICR MS	(Bianco et al., 2018)
$PM_{2.5}$	Changchun		Acetonitrile water	1.17±0.13	1.56±0.11	Orbitrap MS	(Wang et al., 2021)
	Shanghai			1.41±0.19	1.85±0.04		
	Guangzhou			1.48±0.05	1.85±0.02		

Table S4. Comparison of O/C and H/C ratios of CHONS compounds in this study and other studies.

Sample/type	Site/type		Extraction solution	O/C	H/C	Instrument	Ref.
$PM_{2.5}$	CHONS/Guangzhou		Methanol	0.72±0.06	1.72±0.03	FT-ICR MS	This study
rainwater	Northeastern United States		Water	1.7 ±0.9	1.8 ±0.6	FT-ICR MS	(Altieri et al., 2009)
$PM_{2.5}$	Pearl River Delta		Water	0.81 ± 0.22	1.73 ± 0.29	Orbitrap MS	(Lin et al., 2012a)
$PM_{2.5}$	Cambridge	winter	Water and acetonitrile	0.73	1.99	Orbitrap MS	(Rincón et al., 2012)
		summer		0.80	1.65		
Cloud	Colorado		Water	0.44±0.04	1.17±0.10	FT-ICR MS	(Zhao et al., 2013)
				0.43±0.04	1.19±0.11		
PM (0.18-1.8 µm)	California	after midnight		0.99±0.02	1.7±0.0	Orbitrap MS	(O'brien et al., 2014)
		morning		1.0±0.005	1.7±0.0		
		afternoon		0.92±0.03	1.7±0.05		
		before midnight		0.89±0.09	1.7±0.05		
TSP	Virginia		Water	0.71±0.21	1.65±0.20	FT-ICR MS	(Willoughby et al., 2014)
			Pyridine	0.64±0.23	1.52±0.28		
			Acetonitrile	0.45±0.25	1.27±0.29		
$PM_{2.5}$	Beijing	Hazy	DCM	0.69±0.31	1.57±0.37	FT-ICR MS	(Jiang et al., 2016)
		Clear		0.76±0.27	1.75±0.31		
		Hazy	Water	0.70±0.32	1.51±0.37		
		Clear					
$PM_{2.5}$	Wuhan	Winter	Methanol	0.35±0.13	1.58±0.46	Orbitrap MS	(Wang et al., 2016)
		Summer		0.40±0.17	1.69±0.34		
	Nanjing	Summer		0.44±0.21	1.69±0.35		
	Shanghai	Winter		0.42±0.27	1.64±0.52		
		Summer		0.53±0.38	1.64±0.47		
$PM_{2.5}$	Shanghai	Spring	Acetonitrile	0.2	1.5	Orbitrap MS	(Wang et al., 2017)
		Summer		0.4	1.5		
		Fall		0.3	1.6		
		Winter		0.4	1.5		
$PM_{2.5}$	Mainz	low-	Acetonitril	0.91	1.54	Orbitrap	(Wang et

		pollution	e-water			MS	al., 2018)
	Beijing	low-pollution		0.81	1.57		
		high-pollution		0.59	1.56		
Cloud	France		Water	0.23	1.47	FT-ICR MS	(Bianco et al., 2018)
$PM_{2.5}$	Changchun		Acetonitrile-water	1.07±0.11	1.35±0.02	Orbitrap MS	(Wang et al., 2021)
	Shanghai			1.00±0.13	1.56±0.03		
	Guangzhou			0.82±0.03	1.56±0.04		

Table S5. Summary of the calculated molecular characteristics of organosulfur compounds groups detected in source samples, as the FT-ICR MS data are obtained from Cui et al. (2019) and Tang et al. (2020)

		Formula number	MW	H/C	O/C	O/S	DBE	% of (DBE-N) ≥4	% of Xc≥2.5	% of $o/(4s+3n) \geq 1$
BBOA1(Musa)	CHOS	444	360	1.52	0.47	6.21	4.76	57	43	88
	CHONS	371	379	1.55	0.50	7.21	4.98	58	64	64
	Avg/total	815	367	1.53	0.48	6.59	4.85	57	53	77
BBOA2(Hevea)	CHOS	174	396	1.35	0.40	5.97	7.68	69	59	86
	CHONS	65	411	1.56	0.50	7.51	4.79	62	69	63
	Avg/total	239	400	1.40	0.42	6.34	6.98	67	62	80
CCOA1(Anthracite)	CHOS	549	323	1.01	0.40	5.40	8.55	85	82	95
	CHONS	767	340	0.98	0.52	6.49	8.99	94	97	47
	Avg/total	1316	332	0.99	0.47	6.03	8.80	90	91	67
CCOA2(Bituminous coal)	CHOS	463	340	0.99	0.31	4.64	9.90	96	94	85
	CHONS	293	308	0.97	0.49	5.82	8.04	92	93	29
	Avg/total	756	328	0.98	0.38	5.10	9.18	94	93	63
Vehicle emissions	CHOS	112	441	1.31	0.25	4.47	9.54	71	71	75
	CHONS	17	400	1.17	0.72	8.59	6.92	59	59	47
	Avg/total	129	432	1.28	0.35	5.36	8.97	69	69	71
Tunnel aerosols	CHOS	635	325	1.74	0.59	6.79	2.75	46	23	96
	CHONS	410	340	1.81	0.90	8.73	2.78	28	29	91
	Avg/total	1045	331	1.76	0.71	7.53	2.76	39	25	94
Excavator-idling(diesel)	CHOS	1004	353	1.61	0.38	5.81	4.18	68	58	96
	CHONS	310	325	1.47	0. 41	5.59	5.18	56	65	42
	Avg/total	1314	347	1.59	0.38	5.77	4.38	65	60	83
Excavator-moving(diesel)	CHOS	334	326	1.51	0.46	5.20	3.58	54	49	98
	CHONS	117	298	1.62	0.48	5.17	5.55	59	64	9
	Avg/total	451	314	1.35	0.42	5.19	4.38	56	53	75
Excavator-working(diesel)	CHOS	631	342	1.63	0.36	5.44	4.00	62	55	93
	CHONS	260	323	1.47	0.40	5.41	5.26	62	69	27
	Avg/total	891	337	1.58	0.37	5.19	4.35	62	59	74
Diesel-vessels	CHOS	334	306	1.66	0.40	5.14	3.47	55	50	95
	CHONS	13	461	1.50	0.36	6.74	9.38	38	38	46
	Avg/total	347	310	1.66	0.40	5.17	3.60	54	49	93
Heavy-fuel-oil-vessels	CHOS	1110	311	1.48	0.36	4.77	4.85	76	71	83
	CHONS	398	343	1.35	0.39	5.68	6.35	80	86	28
	Avg/total	1508	314	1.47	0.36	4.86	5.00	77	75	68

Table S6. Detailed intensity percentages of isoprene-derived OSs detected at Guangzhou. Noted the formulas in the Table S6-S10 were from the summarization of recent studies and the reference in (Bruggemann et al., 2020; Ye et al., 2020; Zhu et al., 2019; Wang et al., 2019).

Formula $[M\text{-}H]^-$	MW (Da)	DBE	Average RI (‰)
$C_4H_5O_5S^-$	164.9863	2	0.019
$C_4H_7O_5S^-$	167.0020	1	0.067
$C_3H_5O_6S^-$	168.9812	1	0.093
$C_3H_7O_6S^-$	170.9969	0	0.106
$C_4H_5O_6S^-$	180.9812	2	0.049
$C_5H_9O_5S^-$	181.0176	1	0.109
$C_4H_7O_6S^-$	182.9969	1	0.145
$C_3H_5O_7S^-$	184.9761	1	0.200
$C_5H_7O_6S^-$	194.9969	2	0.179
$C_5H_9O_6S^-$	197.0125	1	0.366
$C_3H_3O_8S^-$	198.9554	2	0.372
$C_4H_7O_7S^-$	198.9918	1	0.169
$C_5H_{11}O_6S^-$	199.0282	0	0.191
$C_3H_5O_8S^-$	200.9711	1	0.192
$C_5H_7O_7S^-$	210.9918	2	0.752
$C_5H_9O_7S^-$	213.0074	1	0.482
$C_4H_7O_8S^-$	214.9867	1	0.119
$C_5H_{11}O_7S^-$	215.0231	0	0.141
$C_3H_5O_9S^-$	216.9660	1	0.100
$C_7H_9O_6S^-$	221.0125	3	0.106
$C_8H_{13}O_5S^-$	221.0489	2	0.167
$C_5H_7O_8S^-$	226.9867	2	0.509
$C_5H_9O_8S^-$	229.0024	1	0.170
$C_4H_7O_9S^-$	230.9816	1	0.062
$C_5H_{11}O_8S^-$	231.0180	0	0.030
$C_8H_{11}O_6S^-$	235.0282	3	0.175
$C_7H_9O_7S^-$	237.0074	3	0.703
$C_8H_{13}O_6S^-$	237.0438	2	1.079
$C_8H_{11}O_7S^-$	251.0231	3	0.789
$C_8H_{13}O_7S^-$	253.0387	2	2.206
$C_9H_{15}O_7S^-$	267.0544	2	1.512
$C_8H_{13}O_8S^-$	269.0337	2	0.579
$C_5H_7O_{11}S^-$	274.9715	2	0.036
$C_{12}H_{19}O_6S^-$	291.0908	3	0.206
$C_8H_{13}O_{10}S^-$	301.0235	2	0.061
$C_{12}H_{17}O_8S^-$	321.0650	4	0.139
$C_{10}H_{19}O_{10}S^-$	331.0704	1	0.028
$C_{10}H_{21}O_{10}S^-$	333.0861	0	0.070
$C_{15}H_{31}O_{13}S^-$	451.1491	0	0.035
$C_5H_{10}NO_8S^-$	244.0133	1	0.172
$C_5H_{10}NO_9S^-$	260.0082	1	0.230
$C_5H_8NO_{10}S^-$	273.9874	2	0.099
$C_5H_9N_2O_{11}S^-$	304.9933	2	0.108
$C_8H_{12}NO_{12}S^-$	346.0086	3	0.039

Table S7. Detailed intensity percentages of terpene-derived OSs (including limonene) detected at Guangzhou.

Formula [M-H] $^{-}$	MW (Da)	DBE	Average RI (‰)
$C_6H_{11}O_4S^-$	179.0384	1	0.055
$C_5H_{11}O_6S^-$	199.0282	0	0.166
$C_3H_5O_8S^-$	200.9711	1	0.167
$C_6H_{11}O_6S^-$	211.0282	1	0.348
$C_5H_{11}O_7S^-$	215.0231	0	0.431
$C_9H_{15}O_4S^-$	219.0697	2	0.169
$C_9H_{17}O_4S^-$	221.0853	1	0.189
$C_7H_{11}O_6S^-$	223.0282	2	0.291
$C_9H_{19}O_4S^-$	223.1010	0	0.391
$C_7H_{13}O_6S^-$	225.0438	1	0.462
$C_5H_7O_8S^-$	226.9867	2	0.503
$C_5H_9O_8S^-$	229.0024	1	0.469
$C_9H_9O_5S^-$	229.0176	5	0.471
$C_{10}H_{13}O_4S^-$	229.0540	4	0.478
$C_{10}H_{15}O_4S^-$	231.0697	3	0.453
$C_9H_{15}O_5S^-$	235.0646	2	0.252
$C_8H_{13}O_6S^-$	237.0438	2	0.403
$C_{10}H_{21}O_4S^-$	237.1166	0	0.478
$C_{10}H_9O_5S^-$	241.0176	6	0.630
$C_8H_{17}O_6S^-$	241.0751	0	0.669
$C_6H_{11}O_8S^-$	243.0180	1	0.656
$C_9H_9O_6S^-$	245.0125	5	0.279
$C_{10}H_{15}O_5S^-$	247.0646	3	0.129
$C_9H_{13}O_6S^-$	249.0438	3	0.140
$C_{10}H_{17}O_5S^-$	249.0802	2	0.217
$C_7H_7O_8S^-$	250.9867	4	0.236
$C_8H_{11}O_7S^-$	251.0231	3	0.326
$C_9H_{15}O_6S^-$	251.0595	2	0.507
$C_{10}H_{19}O_5S^-$	251.0959	1	0.771
$C_7H_9O_8S^-$	253.0024	3	0.793
$C_8H_{13}O_7S^-$	253.0387	2	0.912
$C_9H_{17}O_6S^-$	253.0751	1	1.038
$C_{10}H_{21}O_5S^-$	253.1115	0	1.056
$C_9H_7O_7S^-$	258.9918	6	0.416
$C_{10}H_{11}O_6S^-$	259.0282	5	0.290
$C_{10}H_{13}O_6S^-$	261.0438	4	0.062
$C_9H_{11}O_7S^-$	263.0231	4	0.080
$C_{10}H_{15}O_6S^-$	263.0595	3	0.153
$C_8H_9O_8S^-$	265.0024	4	0.189
$C_9H_{13}O_7S^-$	265.0387	3	0.352
$C_{10}H_{17}O_6S^-$	265.0751	2	0.480
$C_8H_{11}O_8S^-$	267.0180	3	0.613
$C_9H_{15}O_7S^-$	267.0544	2	0.799
$C_{10}H_{19}O_6S^-$	267.0908	1	0.910
$C_9H_{17}O_7S^-$	269.0700	1	0.899
$C_7H_{11}O_9S^-$	271.0129	2	0.751
$C_{10}H_9O_7S^-$	273.0074	6	0.313
$C_8H_{17}O_8S^-$	273.0650	0	0.186
$C_{10}H_{15}O_7S^-$	279.0544	3	0.443
$C_9H_{13}O_8S^-$	281.0337	3	0.768

$C_{10}H_{17}O_7S^-$	281.0700	2	0.986
$C_{12}H_{11}O_6S^-$	283.0282	7	1.001
$C_9H_{15}O_8S^-$	283.0493	2	1.067
$C_{10}H_{19}O_7S^-$	283.0857	1	1.150
$C_8H_{13}O_9S^-$	285.0286	2	0.826
$C_{11}H_{15}O_7S^-$	291.0544	4	0.089
$C_9H_{11}O_9S^-$	295.0129	4	0.475
$C_{10}H_{15}O_8S^-$	295.0493	3	0.595
$C_9H_{13}O_9S^-$	297.0286	3	0.737
$C_{10}H_{17}O_8S^-$	297.0650	2	0.834
$C_9H_{15}O_9S^-$	299.0442	2	0.580
$C_{14}H_{23}O_5S^-$	303.1272	3	0.137
$C_{11}H_{17}O_8S^-$	309.0650	3	0.477
$C_{10}H_{15}O_9S^-$	311.0442	3	0.642
$C_{10}H_{17}O_9S^-$	313.0599	2	0.478
$C_{15}H_{25}O_5S^-$	317.1428	3	0.106
$C_{14}H_{23}O_6S^-$	319.1221	3	0.152
$C_{10}H_{15}O_{10}S^-$	327.0391	3	0.358
$C_{14}H_{21}O_7S^-$	333.1013	4	0.129
$C_{15}H_{25}O_6S^-$	333.1377	3	0.164
$C_{10}H_{13}O_{11}S^-$	341.0184	4	0.411
$C_{15}H_{23}O_7S^-$	347.1170	4	0.136
$C_{14}H_{21}O_8S^-$	349.0963	4	0.206
$C_{14}H_{23}O_8S^-$	351.1119	3	0.305
$C_{15}H_{23}O_8S^-$	363.1119	4	0.188
$C_{16}H_{27}O_7S^-$	363.1483	3	0.235
$C_{16}H_{27}O_8S^-$	379.1432	3	0.321
$C_{20}H_{31}O_5S^-$	383.1898	5	0.240
$C_{20}H_{33}O_5S^-$	385.2054	4	0.074
$C_{20}H_{33}O_9S_2^-$	481.1571	4	0.061
$C_{10}H_{16}NO_7S^-$	294.0653	3	1.416
$C_9H_{14}NO_8S^-$	296.0446	3	1.483
$C_{10}H_{16}NO_8S^-$	310.0602	3	0.130
$C_9H_{14}NO_9S^-$	312.0395	3	0.178
$C_{10}H_{16}NO_9S^-$	326.0551	3	0.164
$C_{10}H_{18}NO_9S^-$	328.0708	2	0.274
$C_9H_{16}NO_{10}S^-$	330.0500	2	0.295
$C_{10}H_{16}NO_{10}S^-$	342.0500	3	0.212
$C_{10}H_{15}N_2O_{10}S^-$	355.0453	4	0.153
$C_{15}H_{24}NO_7S^-$	362.1279	4	0.097
$C_{10}H_{17}N_2O_{11}S^-$	373.0559	3	0.201
$C_{14}H_{24}NO_9S^-$	382.1177	3	0.131
$C_{10}H_{17}N_2O_{12}S^-$	389.0508	3	0.066

Table S8. Detailed intensity percentages of other biogenic VOCs-derived OSs (2-Methyl-3-Buten-2-ol; 2-E-pentenal, 2-E-hexenal, 3-Z-hexenal, and cis-3-hexen-1-ol, β-caryophyllene) detected at Guangzhou.

Formula $[M-H]^-$	MW (Da)	DBE	Average RI (‰)
$C_3H_5O_6S^-$	168.9812	1	0.060
$C_4H_9O_5S^-$	169.0176	0	0.069
$C_3H_5O_7S^-$	184.9761	1	0.142
$C_5H_{11}O_6S^-$	199.0282	0	0.264
$C_6H_9O_6S^-$	209.0125	2	0.219

$C_6H_{11}O_6S^-$	211.0282	1	0.607
$C_5H_9O_7S^-$	213.0074	1	0.630
$C_5H_9O_8S^-$	229.0024	1	0.387
$C_9H_{15}O_6S^-$	251.0595	2	0.790
$C_9H_{17}O_7S^-$	269.0700	1	0.910
$C_{14}H_{23}O_5S^-$	303.1272	3	0.140
$C_{15}H_{25}O_5S^-$	317.1428	3	0.110
$C_{14}H_{23}O_6S^-$	319.1221	3	0.199
$C_{14}H_{21}O_7S^-$	333.1013	4	0.191
$C_{15}H_{25}O_6S^-$	333.1377	3	0.201
$C_{15}H_{23}O_7S^-$	347.1170	4	0.190
$C_{14}H_{21}O_8S^-$	349.0963	4	0.135
$C_{14}H_{23}O_8S^-$	351.1119	3	0.336
$C_{15}H_{23}O_8S^-$	363.1119	4	0.237
$C_{16}H_{27}O_7S^-$	363.1483	3	0.289
$C_{16}H_{27}O_8S^-$	379.1432	3	0.419
$C_{15}H_{24}NO_7S^-$	362.1279	4	0.162
$C_{14}H_{24}NO_9S^-$	382.1177	3	0.151

Table S9. Detailed intensity percentages of anthropogenic VOCs-derived OSs detected at Guangzhou.

Formula [M-H] $^-$	MW (Da)	DBE	Average RI (‰)
$C_6H_5O_4S^-$	172.9914	4	0.060
$C_7H_5O_4S^-$	184.9914	5	0.109
$C_7H_7O_4S^-$	187.0071	4	0.120
$C_5H_7O_6S^-$	194.9969	2	0.108
$C_8H_7O_4S^-$	199.0071	5	0.213
$C_7H_5O_5S^-$	200.9863	5	0.216
$C_8H_9O_4S^-$	201.0227	4	0.214
$C_6H_9O_6S^-$	209.0125	2	0.169
$C_7H_{13}O_5S^-$	209.0489	1	0.243
$C_8H_7O_5S^-$	215.0020	5	0.506
$C_9H_{11}O_4S^-$	215.0384	4	0.358
$C_8H_5O_6S^-$	228.9812	6	0.597
$C_9H_9O_5S^-$	229.0176	5	0.574
$C_9H_{11}O_5S^-$	231.0333	4	0.164
$C_9H_{17}O_5S^-$	237.0802	1	0.624
$C_{10}H_{19}O_5S^-$	251.0959	1	1.026
$C_{10}H_{17}O_6S^-$	265.0751	2	0.623
$C_9H_{15}O_7S^-$	267.0544	2	1.043
$C_9H_{17}O_7S^-$	269.0700	1	0.986
$C_{10}H_9O_7S^-$	273.0074	6	0.234
$C_{10}H_{11}O_7S^-$	275.0231	5	0.049
$C_{12}H_{23}O_5S^-$	279.1272	1	0.830
$C_{10}H_{17}O_7S^-$	281.0700	2	1.192
$C_9H_{17}O_8S^-$	285.0650	1	0.473
$C_{11}H_{11}O_7S^-$	287.0231	6	0.312
$C_{11}H_{13}O_7S^-$	289.0387	5	0.062
$C_{10}H_{15}O_8S^-$	295.0493	3	0.651
$C_{10}H_{17}O_8S^-$	297.0650	2	0.669
$C_6H_4NO_6S^-$	217.9765	5	0.061
$C_{10}H_{10}NO_9S^-$	320.0082	6	0.040
$C_{10}H_{16}NO_9S^-$	326.0551	3	0.196

Table S10. Detailed intensity percentages of OSs derived from precursors of multiple sources detected at Guangzhou, including Methyl Vinyl, Methacrolein, glyoxal, methylglyoxal, Oleic acid, and other unsaturated acids, such as Palmitoleic acid, Linoleic acid, Conjugated linoleic acid, 10-Undecenoic acid, as well as some alkanes such as 1-Dodecene.

Formula $[M-H]^-$	MW (Da)	DBE	Average RI (‰)
$C_3H_7O_5S^-$	155.0020	0	0.087
$C_4H_5O_5S^-$	164.9863	2	0.076
$C_4H_7O_5S^-$	167.0020	1	0.588
$C_3H_5O_6S^-$	168.9812	1	0.127
$C_5H_7O_5S^-$	179.0020	2	0.144
$C_5H_9O_5S^-$	181.0176	1	0.719
$C_4H_7O_6S^-$	182.9969	1	0.683
$C_5H_7O_6S^-$	194.9969	2	0.907
$C_6H_{11}O_5S^-$	195.0333	1	1.546
$C_5H_9O_6S^-$	197.0125	1	1.113
$C_3H_3O_8S^-$	198.9554	2	0.004
$C_3H_5O_8S^-$	200.9711	1	0.015
$C_6H_7O_6S^-$	206.9969	3	0.312
$C_7H_{11}O_5S^-$	207.0333	2	0.487
$C_8H_{15}O_4S^-$	207.0697	1	0.392
$C_6H_9O_6S^-$	209.0125	2	2.961
$C_7H_{13}O_5S^-$	209.0489	1	2.110
$C_8H_{17}O_4S^-$	209.0853	0	2.239
$C_5H_7O_7S^-$	210.9918	2	1.181
$C_6H_{11}O_6S^-$	211.0282	1	2.907
$C_7H_{15}O_5S^-$	211.0646	0	0.858
$C_5H_9O_7S^-$	213.0074	1	0.565
$C_4H_7O_8S^-$	214.9867	1	0.002
$C_3H_5O_9S^-$	216.9660	1	0.017
$C_8H_{13}O_5S^-$	221.0489	2	0.742
$C_9H_{17}O_4S^-$	221.0853	1	0.344
$C_8H_{15}O_5S^-$	223.0646	1	3.136
$C_9H_{19}O_4S^-$	223.1010	0	0.657
$C_5H_9O_8S^-$	229.0024	1	0.084
$C_4H_7O_9S^-$	230.9816	1	0.007
$C_9H_{15}O_5S^-$	235.0646	2	5.496
$C_{10}H_{19}O_4S^-$	235.1010	1	0.431
$C_7H_9O_7S^-$	237.0074	3	1.350
$C_8H_{13}O_6S^-$	237.0438	2	4.505
$C_9H_{17}O_5S^-$	237.0802	1	2.513
$C_8H_{15}O_6S^-$	239.0595	1	4.788
$C_5H_9O_9S^-$	244.9973	1	0.006
$C_{10}H_{17}O_5S^-$	249.0802	2	2.914
$C_{11}H_{21}O_4S^-$	249.1166	1	0.448
$C_9H_{15}O_6S^-$	251.0595	2	6.871
$C_{10}H_{19}O_5S^-$	251.0959	1	10.186
$C_9H_{17}O_6S^-$	253.0751	1	4.825
$C_8H_{15}O_7S^-$	255.0544	1	1.826
$C_9H_{19}O_6S^-$	255.0908	0	0.549
$C_{10}H_{17}O_6S^-$	265.0751	2	4.866
$C_{11}H_{21}O_5S^-$	265.1115	1	3.640

$C_8H_{11}O_8S^-$	267.0180	3	2.195
$C_9H_{15}O_7S^-$	267.0544	2	7.408
$C_{10}H_{19}O_6S^-$	267.0908	1	4.505
$C_9H_{17}O_7S^-$	269.0700	1	2.203
$C_8H_{15}O_8S^-$	271.0493	1	0.394
$C_5H_7O_{11}S^-$	274.9715	2	0.006
$C_{13}H_{25}O_4S^-$	277.1479	1	0.545
$C_{10}H_{15}O_7S^-$	279.0544	3	9.100
$C_{11}H_{19}O_6S^-$	279.0908	2	3.420
$C_{12}H_{23}O_5S^-$	279.1272	1	4.561
$C_{11}H_{21}O_6S^-$	281.1064	1	3.002
$C_{10}H_{19}O_7S^-$	283.0857	1	2.828
$C_9H_{17}O_8S^-$	285.0650	1	0.564
$C_{12}H_{19}O_6S^-$	291.0908	3	1.309
$C_{12}H_{21}O_6S^-$	293.1064	2	2.970
$C_{13}H_{25}O_5S^-$	293.1428	1	5.245
$C_{10}H_{15}O_8S^-$	295.0493	3	4.782
$C_{10}H_{17}O_8S^-$	297.0650	2	3.585
$C_{11}H_{21}O_7S^-$	297.1013	1	1.343
$C_{10}H_{19}O_8S^-$	299.0806	1	1.084
$C_9H_{17}O_9S^-$	301.0599	1	0.076
$C_{14}H_{23}O_5S^-$	303.1272	3	0.671
$C_{14}H_{25}O_5S^-$	305.1428	2	1.476
$C_{15}H_{29}O_4S^-$	305.1792	1	0.614
$C_{14}H_{27}O_5S^-$	307.1585	1	6.946
$C_{15}H_{31}O_4S^-$	307.1949	0	1.458
$C_{13}H_{25}O_6S^-$	309.1377	1	2.465
$C_{15}H_{25}O_5S^-$	317.1428	3	0.720
$C_{14}H_{23}O_6S^-$	319.1221	3	1.328
$C_{15}H_{27}O_5S^-$	319.1585	2	1.399
$C_{14}H_{25}O_6S^-$	321.1377	2	2.457
$C_{15}H_{29}O_5S^-$	321.1741	1	7.015
$C_{14}H_{27}O_6S^-$	323.1534	1	2.529
$C_{15}H_{31}O_5S^-$	323.1898	0	0.906
$C_{13}H_{25}O_7S^-$	325.1326	1	1.016
$C_{14}H_{21}O_7S^-$	333.1013	4	1.254
$C_{15}H_{25}O_6S^-$	333.1377	3	1.362
$C_{16}H_{29}O_5S^-$	333.1741	2	1.408
$C_{15}H_{27}O_6S^-$	335.1534	2	2.050
$C_{16}H_{31}O_5S^-$	335.1898	1	6.059
$C_{14}H_{25}O_7S^-$	337.1326	2	2.532
$C_{15}H_{29}O_6S^-$	337.1690	1	2.283
$C_{16}H_{33}O_5S^-$	337.2054	0	1.863
$C_{15}H_{23}O_7S^-$	347.1170	4	1.842
$C_{17}H_{31}O_5S^-$	347.1898	2	1.309
$C_{14}H_{21}O_8S^-$	349.0963	4	1.610
$C_{15}H_{25}O_7S^-$	349.1326	3	2.194
$C_{16}H_{29}O_6S^-$	349.1690	2	2.253
$C_{14}H_{23}O_8S^-$	351.1119	3	2.031
$C_{15}H_{27}O_7S^-$	351.1483	2	2.370
$C_{16}H_{31}O_6S^-$	351.1847	1	5.103
$C_{14}H_{25}O_8S^-$	353.1276	2	1.433
$C_{15}H_{29}O_7S^-$	353.1639	1	1.019

$C_{18}H_{31}O_5S^-$	359.1898	3	0.433
$C_{18}H_{33}O_5S^-$	361.2054	2	1.181
$C_{15}H_{23}O_8S^-$	363.1119	4	1.893
$C_{16}H_{27}O_7S^-$	363.1483	3	1.767
$C_{17}H_{31}O_6S^-$	363.1847	2	1.538
$C_{18}H_{35}O_5S^-$	363.2211	1	3.739
$C_{16}H_{29}O_7S^-$	365.1639	2	3.434
$C_{17}H_{33}O_6S^-$	365.2003	1	3.154
$C_{15}H_{27}O_8S^-$	367.1432	2	1.283
$C_{18}H_{31}O_6S^-$	375.1847	3	0.767
$C_{18}H_{33}O_6S^-$	377.2003	2	1.728
$C_{19}H_{37}O_5S^-$	377.2367	1	2.472
$C_{16}H_{27}O_8S^-$	379.1432	3	1.754
$C_{18}H_{35}O_6S^-$	379.2160	1	2.906
$C_{16}H_{29}O_8S^-$	381.1589	2	1.390
$C_{15}H_{15}O_{10}S^-$	387.0391	8	0.037
$C_{20}H_{37}O_5S^-$	389.2367	2	0.666
$C_{18}H_{31}O_7S^-$	391.1796	3	1.175
$C_{19}H_{35}O_6S^-$	391.2160	2	1.002
$C_{20}H_{39}O_5S^-$	391.2524	1	1.834
$C_{18}H_{33}O_7S^-$	393.1952	2	2.059
$C_{17}H_{31}O_8S^-$	395.1745	2	1.121
$C_{18}H_{35}O_7S^-$	395.2109	1	2.020
$C_{20}H_{37}O_6S^-$	405.2316	2	0.823
$C_{21}H_{41}O_5S^-$	405.2680	1	1.159
$C_{18}H_{31}O_8S^-$	407.1745	3	1.129
$C_{18}H_{33}O_8S^-$	409.1902	2	1.211
$C_{22}H_{41}O_5S^-$	417.2680	2	0.406
$C_{22}H_{43}O_5S^-$	419.2837	1	0.879
$C_{22}H_{41}O_6S^-$	433.2629	2	0.466
$C_{23}H_{45}O_5S^-$	433.2993	1	0.859
$C_{24}H_{45}O_6S^-$	461.2942	2	0.342
$C_{24}H_{47}O_6S^-$	463.3099	1	0.925
$C_{24}H_{45}O_7S^-$	477.2891	2	0.426
$C_5H_8NO_8S^-$	241.9976	2	0.591
$C_6H_{12}NO_8S^-$	258.0289	1	1.249
$C_{10}H_{16}NO_9S^-$	326.0551	3	3.361
$C_9H_{16}NO_{10}S^-$	330.0500	2	0.461
$C_{15}H_{24}NO_7S^-$	362.1279	4	2.253
$C_{14}H_{24}NO_9S^-$	382.1177	3	0.923

Table S11. Number and percentage occurrences of the plausible reactant− product pairs

Type		CHOS − SO_3 → CHO (1)	CHONS − SO_3 → CHON (2)	Total
Number	Median	708	480	1158
	Range	87-1249	48-971	135-2165
	Average±STD	699±324	508±261	1207±578
Percentage(%)	Median	28	20	48
	Range	11-37	5-27	18-62
	Average±STD	27±7	19±6	46±12
Intensity percentages (%)	Median	30	17	49
	Range	10-40	4-29	15-61
	Average±STD	28±7	17±6	46±12

Table S12. Selected meteorological parameters and chemical variables that probably have influences on the formation of NOCs. This table has been revised from our previous study and the references therein (Jiang et al., 2021b).

Abbreviation	Full name	Major Sources/influences
SO_2	Sulfur dioxide	Combustion sources
NO	Nitric oxide	
NO_2	Nitrogen dioxide	
NO_x	Nitrogen oxides	
CO	Carbon monoxide	
O_3	Ozone	Photo-oxidization
NO_x+ O_3	Oxidants	
NH_4^+	Ammonium	Secondary nitrate formation process
NO_3^-	Nitrates	
SO_4^{2-}/nss-SO_4^{2-}	Sulfates/ non-sea-salt sulfates	Secondary sulfate formation process
Cl^-	Chloridion	Sea salt/coal conbustion
K^+/nss-K^+	Potassium/non-sea-salt potassium	Biomass burning (also from coal combustion and other sources)
Levo	levoglucosan	Biomass burning
MTLs	sum of 2-methylthreitol and 2-methylerythritol	Isoprene derived SOA
MSOA	monoterpene-derived secondary organic aerosols	α -/β-pinene derived SOA
FA	Fatty acids	Vehicle emission, coal combustion, cooking, high-level plans
PAHs	Polycyclic aromatic hydrocarbons	Combustion sources
Alkane	Long-chain alkanes with C number from 20 to 36	Combustion sources and high-level plans
ΣSH	steranes and hopanes	Fossil fuels combustion sources
LWC	Liquid water content	Influence the aqueous phase reaction
Tem	Temperature	Influence the gas-to-particle partitioning
RH	Relative humidity	Influence the aqueous phase reaction
OH	Hydroxyl radical	Influence the oxidation state of precursor/ photo-decomposed
pH	potential of hydrogen	Influence the aqueous phase reaction (range: -0.08-4.90)
$\Delta^{14}C$	Radiocarbon isotope	Indicator of fossil or non-fossil sources

Table S13. Number and percentage of compounds classes with significant correlations to the environmental variables.

Type	*p*-value original				*p*-value (FDR-adjusted)			
	CHOS		CHONS		CHOS		CHONS	
Parameters	Positive	Negative	Positive	Negative	Positive	Negative	Positive	Negative
RH	591 (77%)	172 (72%)	180 (23%)	66 (28%)	322 (83%)	20 (74%)	65 (17%)	7 (26%)
Tem	260 (83%)	697 (58%)	54 (17%)	514 (42%)	170 (89%)	352 (57%)	22 (11%)	261 (43%)
MSOA	478 (53%)	465 (88%)	416 (47%)	62 (12%)	375 (58%)	260 (92%)	277 (42%)	22 (8%)
MTLs	336 (73%)	696 (72%)	124 (27%)	274 (28%)	253 (81%)	451 (79%)	60 (19%)	123 (21%)
$\Delta^{14}C$	199 (70%)	440 (69%)	87 (30%)	200 (31%)	37 (71%)	225 (71%)	15 (29%)	92 (29%)
NH_4^+	230 (43%)	244 (85%)	306 (57%)	42 (15%)	21 (26%)	56 (89%)	59 (74%)	7 (11%)
NO_3^-	283 (44%)	159 (79%)	359 (56%)	42 (21%)	46 (36%)	40 (75%)	83 (64%)	13 (25%)
LWC	330 (46%)	22 (72%)	392 (54%)	8 (28%)	17 (100%)	0	43 (100%)	0
pH	65 (56%)	11 (48%)	51 (44%)	12 (52%)	0	0	0	0
H^+	11 (48%)	65 (56%)	12 (52%)	51 (44%)	0	0	0	0
SO_4^{2-}	247 (72%)	131 (63%)	95 (28%)	76 (37%)	0	0	0	0

References

Altieri, K. E., Turpin, B. J., and and Seitzinger, S. P.: Oligomers, organosulfates, and nitrooxy organosulfates in rainwater identified by ultra-high resolution electrospray ionization FT-ICR mass spectrometry, Atmos. Chem. Phys., 2533-2542, doi:10.5194/acp-9-2533-2009, 2009.

Bianco, A., Deguillaume, L., Vaitilingom, M., Nicol, E., Baray, J. L., Chaumerliac, N., and Bridoux, M.: Molecular Characterization of Cloud Water Samples Collected at the Puy de Dome (France) by Fourier Transform Ion Cyclotron Resonance Mass Spectrometry, Environ. Sci. Technol., 52, 10275-10285, doi:10.1021/acs.est.8b01964, 2018.

Bruggemann, M., Xu, R., Tilgner, A., Kwong, K. C., Mutzel, A., Poon, H. Y., Otto, T., Schaefer, T., Poulain, L., Chan, M. N., and Herrmann, H.: Organosulfates in Ambient Aerosol: State of Knowledge and Future Research Directions on Formation, Abundance, Fate, and Importance, Environ. Sci. Technol., 54, 3767-3782, doi:10.1021/acs.est.9b06751, 2020.

Chen, Y. and Bond, T. C.: Light absorption by organic carbon from wood combustion, Atmospheric Chemistry and Physics, 10, 1773-1787, 2010.

Chen, Y., Dombek, T., Hand, J., Zhang, Z., Gold, A., Ault, A. P., Levine, K. E., and Surratt, J. D.: Seasonal Contribution of Isoprene-Derived Organosulfates to Total Water-Soluble Fine Particulate Organic Sulfur in the United States, ACS Earth Space Chem., 5, 2419-2432, doi:10.1021/acsearthspacechem.1c00102, 2021.

Cheng, Y., He, K. B., Engling, G., Weber, R., Liu, J. M., Du, Z. Y., and Dong, S. P.: Brown and black carbon in Beijing aerosol: Implications for the effects of brown coating on light absorption by black carbon, Science of the Total Environment, 599-600, 1047-1055, doi:10.1016/j.scitotenv.2017.05.061, 2017.

Cui, M., Li, C., Chen, Y., Zhang, F., Li, J., Jiang, B., Mo, Y., Li, J., Yan, C., Zheng, M., Xie, Z., Zhang, G., and Zheng, J.: Molecular characterization of polar organic aerosol constituents in off-road engine emissions using Fourier transform ion cyclotron resonance mass spectrometry (FT-ICR MS): implications for source apportionment, Atmos. Chem. Phys., 19, 13945-13956, doi:10.5194/acp-19-13945-2019, 2019.

Dombek, T., Poitras, E., Hand, J., Schichtel, B., Harrington, J. M., and Levine, K. E.: Total sulfur analysis of fine particulate mass on nylon filters by ICP–OES, Journal of Environmental Quality, 49, 762-768, doi:https://doi.org/10.1002/jeq2.20066, 2020.

Frossard, A. A., Shaw, P. M., Russell, L. M., Kroll, J. H., Canagaratna, M. R., Worsnop, D. R., Quinn, P. K., and Bates, T. S.: Springtime Arctic haze contributions of submicron organic particles from European and Asian combustion sources, Journal of Geophysical Research, 116, doi:10.1029/2010jd015178, 2011.

Hawkins, L. N., Russell, L. M., Covert, D. S., Quinn, P. K., and Bates, T. S.: Carboxylic acids, sulfates, and organosulfates in processed continental organic aerosol over the southeast Pacific Ocean during VOCALS-REx 2008, Journal of Geophysical Research, 115, doi:10.1029/2009jd013276, 2010.

Huang, R. J., Yang, L., Cao, J. J., Chen, Y., Chen, Q., Li, Y., Duan, J., Zhu, C., Dai, W., Wang, K., Lin, C., Ni, H., Corbin, J. C., Wu, Y., Zhang, R., Tie, X., Hoffmann, T., O'Dowd, C., and Dusek, U.: Brown Carbon Aerosol in Urban Xi'an, Northwest China: The Composition and Light Absorption Properties, Environmental Science & Technology, 52, 6825-6833, doi:10.1021/acs.est.8b02386, 2018.

Jiang, B., Kuang, B. Y., Liang, Y., Zhang, J., Huang, X. H. H., Xu, C., Yu, J. Z., and Shi, Q.: Molecular composition of urban organic aerosols on clear and hazy days in Beijing: a comparative study using FT-ICR MS, Environ. Chem., 13, 888-901, doi:10.1071/en15230, 2016.
Jiang, H., Li, J., Sun, R., Tian, C., Tang, J., Jiang, B., Liao, Y., Chen, C. E., and Zhang, G.: Molecular Dynamics and Light Absorption Properties of Atmospheric Dissolved Organic Matter, Environ. Sci. Technol., 55, 10268-10279, doi:10.1021/acs.est.1c01770, 2021a.
Jiang, H., Li, J., Chen, D., Tang, J., Cheng, Z., Mo, Y., Su, T., Tian, C., Jiang, B., Liao, Y., and Zhang, G.: Biomass burning organic aerosols significantly influence the light absorption properties of polarity-dependent organic compounds in the Pearl River Delta Region, China, Environ. Int., 144, 106079, doi:10.1016/j.envint.2020.106079, 2020.
Jiang, H., Li, J., Sun, R., Liu, G., Tian, C., Tang, J., Cheng, Z., Zhu, S., Zhong, G., Ding, X., and Zhang, G.: Determining the Sources and Transport of Brown Carbon Using Radionuclide Tracers and Modeling, J. Geophys. Res. Atmos., 126, e2021JD034616, doi:10.1029/2021jd034616, 2021b.
Kuang, B. Y., Lin, P., Hu, M., and Yu, J. Z.: Aerosol size distribution characteristics of organosulfates in the Pearl River Delta region, China, Atmos. Environ., 130, 23-35, doi:10.1016/j.atmosenv.2015.09.024, 2016.
Lin, P., Rincon, A. G., Kalberer, M., and Yu, J. Z.: Elemental Composition of HULIS in the Pearl River Delta Region, China: Results Inferred from Positive and Negative Electrospray High Resolution Mass Spectrometric Data, Environmental Science & Technology, 46, 7454-7462, doi:10.1021/es300285d, 2012a.
Lin, P., Yu, J. Z., Engling, G., and Kalberer, M.: Organosulfates in Humic-like Substance Fraction Isolated from Aerosols at Seven Locations in East Asia: A Study by Ultra-High-Resolution Mass Spectrometry, Environ. Sci. Technol., 46, 13118-13127, doi:10.1021/es303570v, 2012b.
Luk´acs, H., Gelencs´er, A., Hoffer, A., Kiss, G., Horv´ath, K., and Harty´ani, Z.: Quantitative assessment of organosulfates in size-segregated rural fine aerosol, Atmos. Chem. Phys., 9, 231–238, doi:10.5194/acp-9-231-2009, 2009.
O'Brien, R. E., Laskin, A., Laskin, J., Rubitschun, C. L., Surratt, J. D., and Goldstein, A. H.: Molecular characterization of S- and N-containing organic constituents in ambient aerosols by negative ion mode high-resolution Nanospray Desorption Electrospray Ionization Mass Spectrometry: CalNex 2010 field study, J. Geophys. Res. Atmos., 119, 12706-12720, doi:10.1002/2014jd021955, 2014.
Rincón, A. G., Calvo, A. I., Dietzel, M., and and Kalberer, M.: Seasonal differences of urban organic aerosol composition – an ultra-high resolution mass spectrometry study, Environmental Chemistry, 9, 298-319, doi:10.1071/EN12016_AC, 2012.
Schwartz, R. E., Russell, L. M., Sjostedt, S. J., Vlasenko, A., Slowik, J. G., Abbatt, J. P. D., Macdonald, A. M., Li, S. M., Liggio, J., Toom-Sauntry, D., and Leaitch, W. R.: Biogenic oxidized organic functional groups in aerosol particles from a mountain forest site and their similarities to laboratory chamber products, Atmospheric Chemistry and Physics, 10, 5075-5088, doi:10.5194/acp-10-5075-2010, 2010.
Shakya, K. M. and Peltier, R. E.: Investigating missing sources of sulfur at Fairbanks, Alaska, Environ. Sci. Technol., 47, 9332-9338, doi:10.1021/es402020b, 2013.

Shakya, K. M. and Peltier, R. E.: Non-sulfate sulfur in fine aerosols across the United States: Insight for organosulfate prevalence, Atmos. Environ., 100, 159-166, doi:10.1016/j.atmosenv.2014.10.058, 2015.
Stone, E. A., Yang, L., Yu, L. E., and Rupakheti, M.: Characterization of organosulfates in atmospheric aerosols at Four Asian locations, Atmos. Environ., 47, 323-329, doi:10.1016/j.atmosenv.2011.10.058, 2012.
Surratt, J. D., Gómez-González, Y., Chan, A. W. H., Vermeylen, R., Shahgholi, M., Kleindienst, T. E., Edney, E. O., Offenberg, J. H., Lewandowski, M., Jaoui, M., Maenhaut, W., Claeys, M., Flagan, R. C., and Seinfeld, J. H.: Organosulfate Formation in Biogenic Secondary Organic Aerosol, J. Phys. Chem. A, 112, 8345-8378, doi:10.1021/jp802310p, 2008.
Tang, J., Li, J., Su, T., Han, Y., Mo, Y., Jiang, H., Cui, M., Jiang, B., Chen, Y., Tang, J., Song, J., Peng, P. a., and Zhang, G.: Molecular compositions and optical properties of dissolved brown carbon in biomass burning, coal combustion, and vehicle emission aerosols illuminated by excitation–emission matrix spectroscopy and Fourier transform ion cyclotron resonance mass spectrometry analysis, Atmos. Chem. Phys., 20, 2513-2532, doi:10.5194/acp-20-2513-2020, 2020.
Tolocka, M. P. and Turpin, B.: Contribution of organosulfur compounds to organic aerosol mass, Environ. Sci. Technol., 46, 7978-7983, doi:10.1021/es300651v, 2012.
Vogel, A. L., Schneider, J., Muller-Tautges, C., Phillips, G. J., Pohlker, M. L., Rose, D., Zuth, C., Makkonen, U., Hakola, H., Crowley, J. N., Andreae, M. O., Poschl, U., and Hoffmann, T.: Aerosol Chemistry Resolved by Mass Spectrometry: Linking Field Measurements of Cloud Condensation Nuclei Activity to Organic Aerosol Composition, Environ Sci Technol, 50, 10823-10832, doi:10.1021/acs.est.6b01675, 2016.
Wang, K., Zhang, Y., Huang, R.-J., Cao, J., and Hoffmann, T.: UHPLC-Orbitrap mass spectrometric characterization of organic aerosol from a central European city (Mainz, Germany) and a Chinese megacity (Beijing), Atmospheric Environment, 189, 22-29, doi:10.1016/j.atmosenv.2018.06.036, 2018.
Wang, K., Zhang, Y., Huang, R. J., Wang, M., Ni, H., Kampf, C. J., Cheng, Y., Bilde, M., Glasius, M., and Hoffmann, T.: Molecular Characterization and Source Identification of Atmospheric Particulate Organosulfates Using Ultrahigh Resolution Mass Spectrometry, Environ. Sci. Technol., 53, 6192-6202, doi:10.1021/acs.est.9b02628, 2019.
Wang, K., Huang, R.-J., Brüggemann, M., Zhang, Y., Yang, L., Ni, H., Guo, J., Wang, M., Han, J., Bilde, M., Glasius, M., and Hoffmann, T.: Urban organic aerosol composition in eastern China differs from north to south: molecular insight from a liquid chromatography–mass spectrometry (Orbitrap) study, Atmos. Chem. Phys., 21, 9089-9104, doi:10.5194/acp-21-9089-2021, 2021.
Wang, X., Hayeck, N., Brüggemann, M., Yao, L., Chen, H., Zhang, C., Emmelin, C., Chen, J., George, C., and Wang, L.: Chemical Characteristics of Organic Aerosols in Shanghai: A Study by Ultrahigh-Performance Liquid Chromatography Coupled With Orbitrap Mass Spectrometry, J. Geophys. Res. Atmos., 122, 11703-11722, doi:10.1002/2017jd026930, 2017.
Wang, X. K., Rossignol, S., Ma, Y., Yao, L., Wang, M. Y., Chen, J. M., George, C., and Wang, L.: Molecular characterization of atmospheric particulate organosulfates in three megacities at the middle and lower reaches of the Yangtze River, Atmos. Chem. Phys., 16, 2285–2298, doi:10.5194/acp-16-2285-2016, 2016.

Willoughby, A. S., Wozniak, A. S., and Hatcher, P. G.: A molecular-level approach for characterizing water-insoluble components of ambient organic aerosol particulates using ultrahigh-resolution mass spectrometry, Atmos. Chem. Phys., 14, 10299-10314, doi:10.5194/acp-14-10299-2014, 2014.
Yassine, M. M., Harir, M., Dabek-Zlotorzynska, E., and Schmitt-Kopplin, P.: Structural characterization of organic aerosol using Fourier transform ion cyclotron resonance mass spectrometry: aromaticity equivalent approach, Rapid Commun. Mass Spectrom., 28, 2445-2454, doi:10.1002/rcm.7038, 2014.
Ye, Y., Zhan, H., Yu, X., Li, J., Wang, X., and Xie, Z.: Detection of organosulfates and nitrooxy-organosulfates in Arctic and Antarctic atmospheric aerosols, using ultra-high resolution FT-ICR mass spectrometry, Sci. Total Environ., 767, 144339, doi:10.1016/j.scitotenv.2020.144339, 2020.
Zhao, Y., Hallar, A. G., and Mazzoleni, L. R.: Atmospheric organic matter in clouds: exact masses and molecular formula identification using ultrahigh-resolution FT-ICR mass spectrometry, Atmos. Chem. Phys., 13, 12343-12362, doi:10.5194/acp-13-12343-2013, 2013.
Zhu, M., Jiang, B., Li, S., Yu, Q., Yu, X., Zhang, Y., Bi, X., Yu, J., George, C., Yu, Z., and Wang, X.: Organosulfur Compounds Formed from Heterogeneous Reaction between SO2 and Particulate-Bound Unsaturated Fatty Acids in Ambient Air, Environ. Sci. Technol. Lett., 6, 318-322, doi:10.1021/acs.estlett.9b00218, 2019.